# Networked Motion Control for Smart EV with multiple-package transmissions and time-varying network-induced delays

Wanke Cao, Jizhi Liu, Jianwei Li, Qingqing Yang, and Hongwen He



**Original citation & hyperlink:**
Cao, W., Liu, J., Li, J., Yang, Q. and He, H., 2021. Networked Motion Control for Smart EV with multiple-package transmissions and time-varying network-induced delays. *IEEE Transactions on Industrial Electronics* (In press)
https://dx.doi.org/10.1109/TIE.2021.3070499

DOI 10.1109/TIE.2021.3070499
ISSN 0278-0046
ESSN 1557-9958

Publisher: IEEE

This article has been accepted for publication in a future issue of this journal, but has not been fully edited. Content may change prior to final publication. Citation information: DOI 10.1109/TIE.2021.3070499, IEEE Transactions on Industrial Electronics

# Networked Motion Control for Smart EV with multiple-package transmissions and time-varying network-induced delays

*Wanke Cao Member, IEEE, Jizhi Liu, Jianwei Li* Member, IEEE, Qingqing Yang Member, IEEE, Hongwen He Senior Member IEEE*

***Abstract*: This paper aims to address the coupled problem of the multiple-package transmissions (MPT) and time-varying network-induced delays (TND) within the networked motion control systems of smart electric vehicles (EVs). The recent development of advance digital sensors, actuators and controllers leverage the worldwide upgrade of transportation in terms of electrification and intellectualization. However, for smart EVs, this updating may challenge the in-vehicle network and then the vehicle control performance. In particular, the non-synchronous MPT and the TND are the key issues in the vehicle's integrated motion control due to the absence of the synchronization mechanism and limitation of communication bandwidth. To deal with the effects of coupled MPT and TND, a hybrid schedule-control framework (HSCF) is developed, where a new multiple-package transmissions scheduler is developed with a flexible time-triggered schedule strategy with fractional-type basic period to eliminate the effect of the MPT and reorganize the TND to a bounded range of delay. Furthermore, an H∞-based linear quadratic regulator (LQR) control approach is designed to deal with the uncertainties caused by the time-varying network-induced delays as well as guarantee the system's stability. The effectiveness of the proposed scheme is verified in three cases by the real-time hardware-in-the-loop (HIL) bed tests.**

***Index Terms*—Smart electric vehicle, motion control, multiple-package transmission, network induced delay, hybrid schedule-control scheme.**

## I. Introduction

With the increasing development of industrial electronic technologies, worldwide transportation electrification is a key solution for decarbonizing the road transport sector [1-5]. Especially, in recent years, with advanced power electronic and measuring devices, the electric motor's advantages in terms of torque generation and measurement have been successfully explored, e.g., the fast and accurate torque response and measurement of these electric motors, which bring great potential for the electrification and intellectualization updating of the road electric vehicles (EVs) [6]. Emerging multi-wheel-independent-drive EVs, in which each wheel is driven by an electric motor to enhance vehicle dynamic and energy conservation have been rapidly developed in the last decades [6-13]. The examples include a variety of prototype vehicles with in-wheel motors including the Audi e-Tron by Audi AG [14] etc. Some commercial vehicles, e.g., the "K9" electric buses with simplified two-electric-motor-independent-drive technologies developed by the BYD Ltd [15], are running in Guangzhou province, China. However, few high-speed EVs with multiple in-wheel motors can be found running on the road due to some key challenges, such as high cost, reliability and safety problems [16-18]. These problems have been drawing a significant interest from both the industry and academia [19, 20]. In recent years, the motion control of high-speed smart EVs has been one of the focuses, and various integrated motion control technologies have been proposed to strengthen the vehicle's motion safety, e.g., integrated anti-slip control (ASC) and direct yaw-moment control (DYC) [5], integrated active front-wheel steering (AFS) and DYC [21], integrated roll angle control (RAC) and DYC [22], integrated advanced driver assistant system (ADAS) and DYC, etc. [23, 24].

The integrated motion control systems within the EVs require the increasing usage of sensors and actuators, which lead to a large amount of real-time data being exchanged synchronously. Instead of traditional point-to-point wires, the in-vehicle networks, e.g., control area network (CAN), have been utilized widely in modern EVs, as shown in Fig. 1. The networked motion control systems possess several advantages, including less wiring, lower cost, and more maintainability of the system [21, 25-28]. However, compared with the traditional centralized control systems, there are several main weakness or constrains within the in-vehicle networked systems based on CAN, as following: (1) the distribution of network nodes, including digital sensors, controllers and actuators, which are placed in different locations and run on event/time-driven mode, respectively; (2) the absence of the synchronization mechanism within the distributed systems, that is, the clock of the distributed nodes may not be synchronous; (3) the limitation of communication bandwidth over CAN, that is, the message transmissions over CAN bus are non-time-critical transmissions and are the exploitation of its native distributed arbitration mechanism. These problems would lead to the non-synchronous multiple-package transmissions (MPT) and time-varying network-induced delays (TND). According to the studies[21, 29], the effect of MPT or TND is one of the reasons that degrades the system performance or even makes the system unstable.

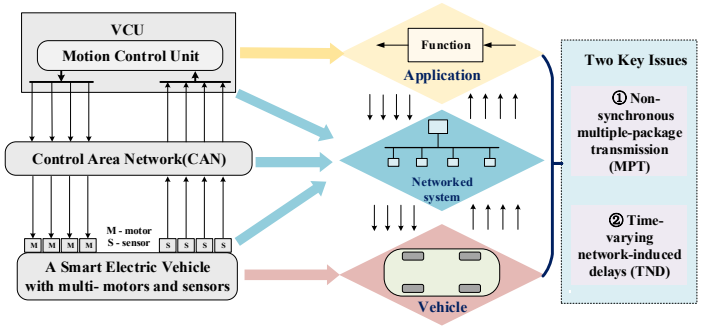


Fig. 1 Networked motion control for a smart EV with multi-motors

Some recent studies focus on the development of robust algorithms against the negative influence of the TND to ensure vehicle motion stabilization [21, 22, 26, 30]. Shuai et al. [21] demonstrated that the time-varying delays induced by CAN in the forward channel could degrade the vehicle yaw motion performances for an EV with four in-wheel motors. Zhu et al. [26] discussed furtherly the influence of the network induced delays caused by CAN in both the feedback and forward channels with two homogenous Markov chains and proposed a delay-dependent linear quadratic regulator (LQR) controller to guarantee the vehicle yaw

All of the authors are with the School of Mechanical Engineering, Beijing Institute of Technology, Beijing, China(Corresponding Author: Jianwei Li)

motion stabilization. Li et al. [31] considered the coupling effects of CAN-induced time-varying delays and event-driven manner of the controller nodes and developed a robust controller to suppress the oscillations for integrated motor-transmission (IMT) system during vehicle speed tracking. Cao et al. [30] presented a fuzzy-based sliding-mode controller (SMC) to enhance the robustness of the lateral motion control system for an EV with four in-wheel motors, subject to the CAN-induced delays. However, the multiple-package transmissions problem are ignored in the aforementioned studies.

Also, regarding to the influence of the multiple-package transmissions on the real-time control systems, several published studies can be found in the open knowledge filed. Li et al. [32] investigated the problem of finite-time state estimation error for delayed periodic neural networks due to the MPT. Li et al. [33] also discussed the instability of the networked control systems (NCS) caused by the multiple-packet transmission policy and proposed a sliding-mode predictive controller. Shuai et al. [29] discussed the instability of EVs with four in-wheel motors owing to the MPT in the forward channel, where the driving force control commands were separately transferred from the vehicle control unit (VCU) to the actuators in four packets. Cao et al. [27] ~~gives~~ present a simplified and practical scheme to deal with the multiple package transmission activities in both the forward and feedback channels by introducing a "time-buffer" adding to the feedback channel. The "time-buffer" is defined as "a period of time" that is used to deal with the message asynchrony in the multiple-package transmissions [27]. However, the applications of the time buffer and the long-data frame may cause longer time delays artificially. The previous approaches can hardly meet the increasing requirements of the EV electrification updating with multi-systems (such as DYC/AFS/ABS).

Combining the above two aspects of literature, most previous studies consider and address one aspect of the influence of the network. Therefore, the main contributions of this study are summarized as follows:

- A hybrid schedule-control framework (HSCF) for the networked motion control is proposed, under which a scheduler and a controller are actively hybridized to change the information flows as well as to deal with the uncertainties caused by the bounded time-varying delays.
- A new scheduling approach is developed by a novel introducing of a flexible time triggered scheduler with the fractional-type basic period (FBP) to eliminate the effect of the MPT and reorganize the TND to a bounded range of time-varying delays. Also, a robust control is developed to guarantee the stability of the closed-loop system along with the multiple-package transmissions scheduling.

The effectiveness of the proposed scheme is verified in three different typical cases in hardware-in-the-loop (HIL) experimental tests with a real-time digital vehicle simulator and a real prototypical network system.

The remainder of this paper is organized as follows. In Section II, a typical networked motion control architecture for the integrated ASC and DYC system is presented. In Section III, the HSCF is proposed. Also, the integrated scheduler and controller are designed and analysed in detail. The experimental results with the real-time digital vehicle simulator and real prototypical network system are discussed in Section IV. Finally, conclusions are provided in Section V.

## II. System Description

### A. Networked Motion Control Architecture for EVs

A typical networked motion control architecture of the integrated ASC and DYC system for a smart EV with four in-wheel motors is illustrated in Fig.2. It mainly consists of a VCU, the CAN, multiple actuators (e.g. four in-wheel motors, motor controllers) and multiple sensors (e.g. speed or torque sensors, the yaw rate sensor, the longitudinal or lateral acceleration sensor, etc.), among others. The integrated motion control strategy is implemented in the VCU, which includes a motion control unit based on DYC, a reference state model, parameter estimation with the maximum transmissible torque estimation (MTTE) [34] and a torque distribution unit (TDU) where both ASC and DYC are considered synthetically. The sensors send the state signals to VCU through CAN, and the VCU calculates the control commands then sends them to the actuators. It is obvious that the integrated ASC and DYC system for the EV with four in-wheel motors is a typical networked motion control system with multiple sensors and multiple actuators. ( $\delta_f$ is the front wheel steering angle, $\beta_{ref}$ is the reference sideslip angle, $\gamma_{ref}$ is the reference yaw rate, $\beta$ is the sideslip angle, $\gamma$ is the yaw rate, $M_z$ is the yaw-moment command imposed to the vehicle, $\omega_{mi}$ denotes each motor speed, $T_{wi}^*$ denotes torque command of each motor.)

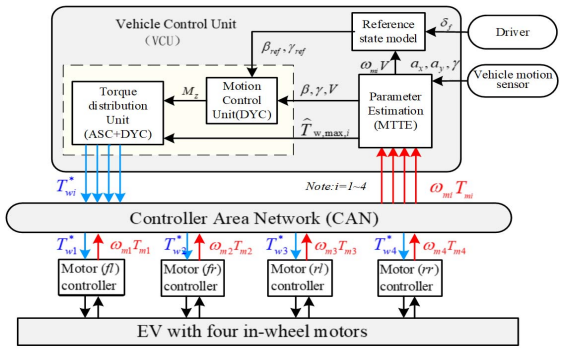


Fig. 2. A typical networked control architecture for the EVs over CAN

### B. Analysis of the network induced uncertainties

The in-vehicle network, dealing with data exchange among the VCU, sensors and actuators, may lead to the following issues: (1) the multiple-package transmissions, that is, the sensor or actuator data are transmitted in several separate network packets due to the devices being distributed in different sub-systems and the absence of synchronization mechanism within the system. Generally, in a distributed control system with multiple inputs and multiple outputs, it is reasonable to assume that the network nodes (digital sensors, controllers and actuators) work on time-driven mode where a node runs periodically according to its local clock. However, their clocks may not be synchronous, which leads to non-synchronous MPT. (2) the TND owing to the limitation of communication bandwidth over CAN. The message transmissions over CAN bus need to obtain the right to use the bus through Carrier Sense Multiple Access (CSMA) arbitration mechanism because of limited carrying capacity and communication bandwidth. Furthermore, the message transmissions over CAN bus are non-time-critical transmissions, and the time delays may be unknown and time-varying, which leads to uncertainties. For example, the sensor-to-controller delay $\tau_{sc}$ and the controller-to-actuator delay $\tau_{ca}$, as shown in Fig. 3, will inevitably occur while exchanging data among devices connected to the shared network medium. These problems, sometimes, may also couple to each other, degrade the control performance and even destabilize the system [27, 29, 35]

For example, for a control system with multiple inputs and multiple outputs, the time-driven mode where a node periodically

This article has been accepted for publication in a future issue of this journal, but has not been fully edited. Content may change prior to final publication. Citation information: DOI 10.1109/TIE.2021.3070499, IEEE Transactions on Industrial Electronics



runs is generally adopted in all the components (digital sensors, controllers and actuators). The dotted curves in Fig. 3 represent the actual system states that change with time, and the $x_{1,2,3,4}$ represent the actual system states at the time of sampling. The network induced delay in the feedback-control loop is $\tau_{loop}$. Owing to the distribution of network nodes, the absence of a synchronization mechanism within the system and the limitation of communication bandwidth, the network-induced delays in the closed-loop system may be described approximately as $\tau_{loop} = \tau_{sc} + \tau_{ca} \approx 2T$, $T$ is the system sampling period, along with the unsynchronized sampling and execution behaviours, as shown in Fig.3. These problems make the control system design difficult and even lead to system instability.

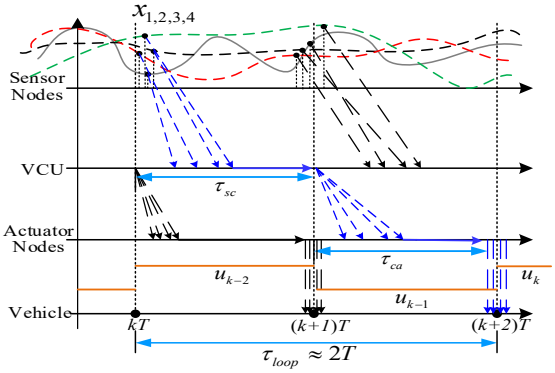


Fig. 3. Communication information flow without the scheduler.

## III. Networked Motion Control with a New Scheduler

In order to solve problems caused by the application of the in-vehicle network, a new HSCF as shown in Fig. 4 is proposed in this section. In the proposed framework, a new network scheduler, as shown as in Fig.5, is developed to deal with the communication information flows. Moreover, a robust motion controller is designed to generate the desired reference driving force commands, to improve the vehicle motion performance and guarantee the system robust stability in the following.

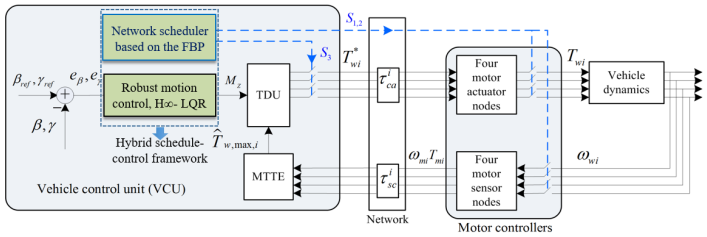


Fig. 4. The hybrid schedule-control framework.

### A. The New Scheduler Design

To deal with the aforementioned uncertainties, e.g., the unsynchronized and delayed sampling or execution behaviours caused by the MPT and the TND in both forward and feedback channels, a new scheduler is presented in this section, where a flexible time triggered scheduling strategy based on the FBP is employed.

Firstly, an available flex time-triggered protocol designed on the basis of the native Media Access Control (MAC) protocol of CAN, e.g., Flex-CAN protocol as in [36], is adopted in this study, where the transmissions of information packets are organized with basic periods, as shown in Fig.5.

Secondly, the sample period of the control system with the size of $T$ is divided into $n$ basic periods, that is, so-called the fraction-type basic period, and the fractional-type basic period is defined with a size of $T/n$. For example, in a simplified design, setting $i$=2, then $n = 2^i = 4$, that is one sample period is divided into four basic periods, as shown in Fig.5. The message packets are assigned to the basic periods, and all message packets are transferred in corresponding basic periods, which ensure the deterministic and real-time of message transmissions.

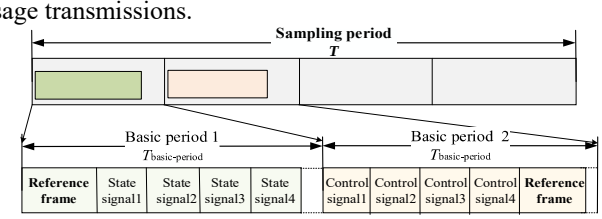


Fig. 5. Scheduling strategy with a basic period

Thirdly, the scheduling strategy based on the FBP has the characteristic of application-oriented synchronization (the control loops involving sensors, controller and actuators) to meet more stringent levels of dependability. The basic period 1 is utilized for the MPT of the sampling signals from sensors to controller in the feedback channel, which is so-called the sampling basic period (SBP). The SBP includes a reference frame and four state signals. To guarantee the synchronized sampling behaviors of multiple sensors, all sensors are triggered by a reference frame to send the state signals in the SBP. The basic period 2 is used for the MPT of command signals from VCU to actuators in the forward channel, which is so-called the command basic period (CBP). The CBP includes four control signals and a reference frame. Similarly, to guarantee the synchronized execution behaviours of four in-wheel motors, all actuators are triggered by a reference frame to perform the received commands in the CBP. The reference frames are sent by the scheduler with the highest priority. With the SBP, the CBP and the scheduler, the MPT problems in both feedback and forward channels are dealt with, e.g., the entire loop delay (see the $\tau_{loop}$) is reduced and the actions of sending multiple state signals or implementing the multiple command signals are synchronized.

To highlight the advances of the proposed FBP based scheduling approach, a comparison between the new scheduler and the previous time-buffer based method [27] is made as show in the Fig. 6. With the previously proposed method, to deal with the state signal asynchrony occurring in the feedback channel from the sensors to VCU, a time buffer with the size $T_b$ is introduced, which will lead to longer delay as shown in Fig. 6. (a). Meanwhile, to cope with the command signal asynchrony occurring at actuator ends in the forward channel, the VCU broadcasts a long command frame with four command signals loaded, and thus all the controllers simultaneously receive and implement the commands once the long command frame arrives. Whereas, with the proposed new scheduler, as shown in Fig. 6 (b), all the state signals are sent in the designated fractional-type basic period. Then the VCU broadcasts 4 short frames and a reference frame in the following designated fractional-type basic period, and all the motor controllers receive and implement the commands once the reference frame arrives.

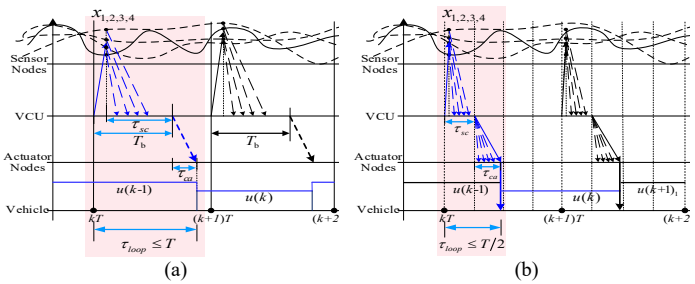


Fig. 6 The message flow in (a) the previous feedback-control loop[27];

(b) the proposed fractional-type basic period based feedback-control loop

The results show that with the proposed scheme the unsynchronized behaviors of multiple sensors and execution behaviors of multiple actuators are explicitly eliminated. And the network induced delay in the feedback control loop is also reduced to a bounded range, as shown in Eq. 1.

$$\tau_{loop} = \tau_{sc} + \tau_{ca} \le T/2 \tag{1}$$

**Remark 1:** To ensure that all message packets in SBP or CBP are successfully transferred, the size of designed basic period has to meet the following schedulable inequality:

$$\sum (T_{message}^{\max})] < T_{base-period} \tag{2}$$

where

$$T_{message}^{\max} = \left( \left[ \frac{g + 8d_j - 1}{4} \right] + g + 10 + 8d_j \right) \Big/ f_{baud},$$
$$with\ g = \begin{cases} 34, \text{for standard frame} \\ 54, \text{for extended frame} \end{cases},\ d_j \le 8$$

with $T_{message}^{\max}$ being the maximum physical transmission time of one message packet [37]; $T_{base-period}$ being the size of the basic period, $f_{baud}$ being the network baud rate; $d_j$ being the data length of a packet; $\sum (T_{message}^{\max})$ being the maximum time to transmit all frames in the basic period; $\left[ (g + 8d_j - 1)/4 \right]$ being the maximum number of the stuff bits; g being the number of bits of the fixed parts related to bit stuff, which is 34 for a standard frame and 54 for an extended frame; number 10 being the number of bits of the fixed parts not related to bit stuff. The numbers in Eq. 2 are obtained according to CAN2.0B protocol [38] .

### *B. Control-Oriented Model for Vehicle Lateral Dynamics*

To improve the vehicle yaw motion tracking performance, it should keep the actual motion states, e.g., the sideslip angle $\beta$ and the yaw rate $\gamma$ , tracking the reference states, e.g., the reference sideslip angle and the reference yaw rate $\gamma_{ref}$ , with the help of the yaw moment $M_z$.

Firstly, a widespread expression of the reference state model is considered as shown in Eq.3, where the desired/reference sideslip angle is selected to be zero, whereas the desired/reference yaw rate is usually defined by the steering angle, the vehicle speed and the structure parameters [26, 27].

$$x_{ref} = \frac{1}{1 + \tau_\gamma s} R\delta_f \tag{3}$$

where

$$x_{ref} = \left[ \beta_{ref} \quad \gamma_{ref} \right]^T, R = [0 \quad V \Big/ \left( l_f + l_r + \frac{mV^2 (C_r l_r - C_f l_f)}{2C_f C_r (l_f + l_r)} \right) ]^T$$

$\tau_\gamma$ is the time constants of the desired yaw rate. $C_f$ and $C_r$ denote the cornering stiffness of the front and rear tires, respectively.

The system model of the lateral dynamics of a vehicle with DYC can be seen in [27].

The system model with the reference model as in Eq. 3 can be rewritten as the discrete-time equations in Eq. 4:

$$\begin{aligned} x(k+1) &= A_d x(k) + B_d u(k) + E_d \delta_f(k) \\ x_{ref}(k+1) &= A_{refd} x_{ref}(k) + R_{refd} \delta_f(k) \end{aligned} \tag{4}$$

where

$$A_d = e^{AT} \quad B_d = \int_0^T e^{As} B ds \quad E_d = \int_0^T e^{As} E ds$$
$$A_{refd} = e^{A_{ref} T} \quad R_{refd} = \int_0^T e^{A_{ref} s} R_{ref} ds$$

where

$$A = \begin{bmatrix} \frac{-2(C_f + C_r)}{mV} & \frac{-2(C_f l_f - C_r l_r)}{mV^2} - 1 \\ \frac{-2(C_f l_f - C_r l_r)}{I_z} & \frac{-2(C_f l_f^2 + C_r l_r^2)}{I_z V} \end{bmatrix} \quad B = \begin{bmatrix} 0 \\ \frac{1}{I_z} \end{bmatrix}$$
$$E = \begin{bmatrix} \frac{2C_f}{mV} \\ \frac{2C_f l_f}{I_z} \end{bmatrix} \quad A_{ref} = \begin{bmatrix} 0 & 0 \\ 0 & -\frac{1}{\tau} \end{bmatrix} \quad R_{ref} = R$$

with $T$ being the sampling period of the motion control system.

Secondly, a new vector $e$ is defined as Eq. 5:

$$e = x - x_{ref} = [\beta - \beta_{ref} \quad \gamma - \gamma_{ref}]^T \tag{5}$$

Substituting Eq. 5 into Eq. 4, the discrete-time model of the vehicle tracking control can be described as:

$$e(k+1) = \overline{A}_d e(k) + \overline{B}_d u(k) + \overline{G}_d \delta'(k) \tag{6}$$

where

$$\overline{A}_d = A_d,\ \overline{B}_d = B_d, \delta'(k) = [\delta(k) \ x_{ref}^T(k)]^T$$
$$\overline{E}_d = E_d - R_{refd},\ \overline{F}_d = A_d - A_{refd}, \overline{G}_d = \left[ \overline{E}_d \quad \overline{F}_d \right]$$

### *B. Analysis of the uncertainties caused by the in-vehicle network*

Furtherly, considering the effect of the in-vehicle network, the proposed fractional-type basic period is employed, for example, setting *i*=2, then $n = 2^i = 4$. And the fractional-type basic period is defined with a size of *T*/4 according to (1), and the time-varying network induced delay in the loop is bounded as $\tau_{loop} \in (0, T/2]$ .

With the time-varying network-induced delays, the model of the close-loop system is reconstructed as shown in Eq.7.

$$u(t) = \begin{cases} u(k-1), t \in [kT, kT + \tau_k] \\ u(k), t \in [kT + \tau_k, (k+1)T] \end{cases},\ k = 0, 1, 2... \tag{7}$$

Due to the loop delay $\tau_{loop} < T$ , the discrete-time model of the closed-loop system can be derived as shown in Eq. 8.

$$e(k+1) = \overline{A}_d e(k) + \overline{B}_d u(k) + \Gamma_1(\tau_k)\left(u(k-1) - u(k)\right) + \overline{G}_d \delta_f' \tag{8}$$

where

$$\Gamma_1(\tau_k) = \int_{T-\tau_k}^{T} e^{As} ds B$$

Defining a new vector $\xi(k) = [e^T(k) \ u(k-1)]^T$ , an an augmented delay system equation can be obtained as:

$$\xi(k+1) = A_{aug} \xi(k) + B_{aug} u(k) + G_{aug} \delta_f'(k) \tag{9}$$

where

$$A_{aug} = \begin{bmatrix} e^{AT} & \Gamma_1(\tau_k) \\ 0 & 0 \end{bmatrix}, \quad B_{aug} = \begin{bmatrix} \overline{B}_d - \Gamma_1(\tau_k) \\ I \end{bmatrix}, \quad G_{aug} = \begin{bmatrix} \overline{G}_d \\ 0 \end{bmatrix}$$

The time-varying loop delays bring about uncertainties to the control system, e.g., the uncertain term $\Gamma_1(\tau_k)$ in the system matrix $A_{aug}$ and $B_{aug}$ as shown in (9). The uncertain term $\Gamma_1(\tau_k)$ can be linearized by Taylor Series Expansion and then expressed as a polytope of matrices.

The Taylor Series Expansion of the Uncertainties $\Gamma_1(\tau_k)$ can be expressed as:

$$\Gamma_1(\tau_k)=\int_{T-\tau_k}^{T} e^{As}dsB=-\sum_{q=1}^{\infty}\left(-\tau_k\right)^q\frac{A^{q-1}}{q!}e^{AT}B \tag{10}$$

Then, $\Gamma_1(\tau_k)$ can be expressed as a finite summation and a remainder as following:

$$\Gamma_1(\tau_k)=-\sum_{q=1}^{h}\left(-\tau_k\right)^q\frac{A^{q-1}}{q!}e^{AT}B+\Theta^h \tag{11}$$

With a proper selection of the number $h$ and neglecting the remainder $\Theta^h$, $\Gamma_1(\tau_k)$ is approximated as:

$$\Gamma_1(\tau_k)=-\sum_{q=1}^{h}\left(-\tau_k\right)^q\frac{A^{q-1}}{q!}e^{AT}B \tag{12}$$

With defining the notations:

$$\begin{aligned}
&G_q=(-1)^{q+1}\frac{A^{q-1}}{q!}e^{AT}B\\
&\varphi_1=\begin{bmatrix}\underline{\rho}^hI & \underline{\rho}^{h-1}I & \cdots & \underline{\rho}^2I & \underline{\rho}I\end{bmatrix}^T\\
&\varphi_2=\begin{bmatrix}\underline{\rho}^hI & \underline{\rho}^{h-1}I & \cdots & \underline{\rho}^2I & \overline{\rho}I\end{bmatrix}^T\\
&\vdots\\
&\varphi_{h+1}=\begin{bmatrix}\overline{\rho}^hI & \overline{\rho}^{h-1}I & \cdots & \overline{\rho}^2I & \overline{\rho}I\end{bmatrix}^T
\end{aligned} \tag{13}$$

where: $q=1,2,\cdots,h,\underline{\rho}=\tau_{\min}=0,\overline{\rho}=\tau_{\max}=T/2$ , the uncertain term $\Gamma_1(\tau_k)$ can be expressed as the convex matrix polytopes [21]:

$$\begin{aligned}
&\Gamma_1(\tau_k)=\sum_{i=1}^{h+1}\mu_i(k)U_i\\
&\mu_i(k)>0,\sum_{i=1}^{h+1}\mu_i(k)=1,\forall i=1,2\ldots h+1,\forall k\in\mathbb{Z}^+
\end{aligned} \tag{14}$$

where the vertices of the convex polytope can be written as:

$$U_i=\begin{bmatrix}G_h & G_{h-1} & \cdots & G_2 & G_1\end{bmatrix}\varphi_i,\forall i=1,2\ldots h+1 \tag{15}$$

### C. H∞-based LQR controller Design

To deal with the uncertainties and guarantee the robust stability of the networked control system, a robust $H_\infty$-based linear quadratic regulator motion controller is designed, furtherly, in this section.

A performance index *J* function is designed as the quadratic form of the error *e* and the control input *u* as follows.

$$J=\sum_{i=0}^{\infty}(e_i^TQe_i+u_i^TRu_i) \tag{16}$$

With the state-feedback control law $u_k=-K^{'}\xi_k$, the performance index *J* function (16) is also equal to the 2-norm of the following constructed signal:

$$z_k=F\xi_k+Hu(k)=F\xi_k-HK^{'}\xi_k=\left(F-HK^{'}\right)\xi_k \tag{17}$$

where

$$F=\begin{bmatrix}Q^{1/2} & 0\\ 0 & 0\end{bmatrix}\quad;\quad H=\begin{bmatrix}0\\ R^{1/2}\end{bmatrix}$$

Since $\delta'(k)$ is bounded in $l_2=\left\{f:\sum_0^\infty\|f(k)\|^2<\infty\right\}$ space, the $H_\infty$ performance index can be introduced as:

$$J<\eta^2\|\delta'(k)\|_2^2 \tag{18}$$

Combining the functions (10), (18) and (19), the motion controller design problem is transformed into an optimal control problem for the following closed-loop system:

$$\begin{aligned}
&\xi(k+1)=\left(A_{aug}-B_{aug}K\right)^{'}\xi(k)+G_{aug}\delta_f'(k)\\
&z_k=\left(F-HK^{'}\right)\xi_k
\end{aligned} \tag{19}$$

To gain the control law, two lemmas are introduced as follows.

***Lemma 1***: Suppose that the controller is designed. The closed-loop system (19) is stable with a given $H_\infty$ performance $\eta$, if there exists a positive definite matrix $P=P^T>0$, satisfying [21].

$$\begin{bmatrix}
-P & 0 & P\left(A_{aug}-B_{aug}K^{'}\right) & PG_{aug}\\
0 & -I & F-HK^{'} & 0\\
A_{aug}^TP^T & F^T-K^{'T}H^T & -P & 0\\
G_{aug}^TP^T & 0 & 0 & -\eta^2I
\end{bmatrix}<0 \tag{20}$$

The *lemma 1* provides an $H_\infty$ criterion for the closed-loop system, with the proof in APPENDIX B. However, it cannot be directly applied to the controller design due to the bilinear term $P\left(A_{aug}-B_{aug}K^{'}\right)$. The bilinear term can be removed by using a congruence transformation with free matrices being introduced [39],.

***Lemma 2***: Suppose that the controller is designed. The closed-loop system (19) is stable with a given $H_\infty$ performance $\eta$, if there exists a positive definite matrix $\Omega=\Omega^T>0$, *M* satisfying [21, 39].

$$\begin{bmatrix}
-\Omega & 0 & A_{aug}M-B_{aug}K^{'}M & G_{aug}\\
0 & -I & \left(F-HK^{'}\right)M & 0\\
M^TA_{aug}^T-M^TK^{'T}B_{aug}^T & M^T(F^T-K^{'T}H^T) & -\Omega-M-M^T & 0\\
G_{aug}^T & 0 & 0 & -\eta^2I
\end{bmatrix}<0 \tag{21}$$

Defining a new variable $Y=K^{'}M$, then (21) can be transformed into a linear matrix inequality (*LMI*). With the *h*+1 vertices of the convex matrix polytope in (15), conditions in (21) become[21]:

$$\begin{bmatrix}
-\Omega & 0 & A_{aug,i}M-B_{aug,i}Y & G_{aug}\\
0 & -I & FM-HY & 0\\
M^TA_{aug,i}^T-Y^TB_{aug,i}^T & M^TF^T-Y^TH^T & -\Omega-M-M^T & 0\\
G_{aug}^T & 0 & 0 & -\eta^2I
\end{bmatrix}<0 \tag{22}$$

$\forall i=1,2,\ldots,(h+1).$

For given matrices *Q* and *R*, a smaller performance index $\eta$ means that the controlled output *Z* (a combination of the tracking error and the control signal) is also smaller. Therefore, the $H_\infty$-based linear quadratic regulator design can be expressed as [21]:

$$\begin{aligned}
&\min_{\Omega,M,Y,\eta}\ \eta^2\\
&subject\quad to\\
&\begin{bmatrix}
-\Omega & 0 & A_{aug,i}M-B_{aug,i}Y & G_{aug}\\
0 & -I & FM-HY & 0\\
M^TA_{aug,i}^T-Y^TB_{aug,i}^T & M^TF^T-Y^TH^T & -\Omega-M-M^T & 0\\
G_{aug}^T & 0 & 0 & -\eta^2I
\end{bmatrix}<0\\
&\forall i=1,2,\ldots,(h+1).
\end{aligned} \tag{23}$$

The problem described in (23) can be solved with the LMI Toolbox in MATLAB. Then, the $H_\infty$-based linear quadratic regulator design can be obtained by $K^{'}=YM^{-1}$.

## IV. RESULTS AND DISCUSSIONS

### A. Hardware-in-the-loop test

#### 1) Real-time HIL test bed set up with dSPACE

To evaluate the proposed scheme, a real-time hardware-in-loop test bed is constructed with a real-time digital vehicle simulator and

a real prototypical network system as shown in Fig.7. The real-time digital vehicle simulator is implemented by the dSPACE AutoBox simulator with a high-fidelity full-vehicle model. The real prototypical network system consists of a VCU board with a MPC5646 chip, four motor control unit (MCU) boards with S12X chips, two bandwidth competitor unit (BCU) with S12X chips and a CAN bus. A PC is connected to the dSPACE simulator via an ethernet interface to implement experimental operations and show test results.

The main vehicle parameter values used in the real-time HIL bed testes were acquired from a prototype EV by Beijing Electric Vehicle Co., Ltd. and provided in Table 1. The specifications of the four-in-wheel motors in the prototype EV is also given in Table A in Appendix A.

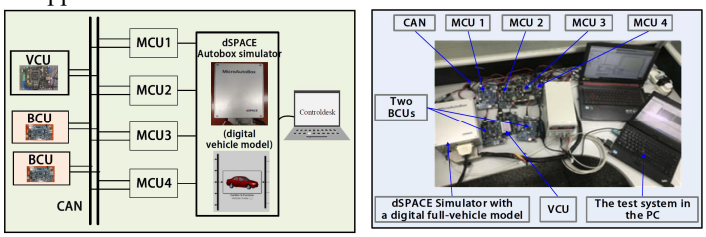


(a) (b)

Fig.7. Real-time test system for networked motion control systems of EVs with 4 IWMs: (a) schematic diagram, (b) hardware systems.

TABLE I. MAIN SYSTEM PARAMETERS

| Symbol | Description | Value/Unit |
|---|---|---|
| $m$ | Vehicle mass | 1050kg |
| $I_Z$ | Vehicle yaw inertia | 1875kg•m$^2$ |
| $l_f$ | Distance from CG to the front axle | 1.000m |
| $l_r$ | Distance from CG to the rear axle | 1.471m |
| $c_f$ | Equivalent cornering stiffness of front tire | 30000N/rad |
| $c_r$ | Equivalent cornering stiffness of front tire | 30000N/rad |
| $i_g$ | Steer gear ratio | 10 |
| $f_{band}$ | Band rate of CAN network | 250/Kbits |
| $d_j$ | Data size in the $j$th message packet | 8/bytes |

2) *Message transmission test*

With the proposed method, the fractional-type basic period is designed with a size of $T/n$ ($n$=4), so the window length of the fractional-type basic period is chosen as $T$/4. The system sampling period is set as $T$=0.02s. The message transmission behaviours over CAN with the TureTime status window are shown in Fig.8.

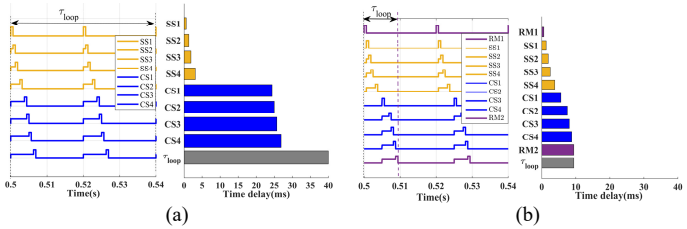


(a) (b)

Fig. 8. The message transmission behaviours: (a) with the traditional none-network-scheduling scheme, (b) with the proposed scheduling scheme.

The orange lines and the blue lines represent the message transmission behaviours of the state signal (SS) and the control signal (CS), respectively, and the purple lines represent the message transmission behaviours of the reference messages, e.g., RM1, RM2. Correspondingly, the orange and blue bars represent the time delay values of the state signals and the control signals being processed and exchanged over CAN relative to the sampling time, respectively. The purple bars represent the time delay values of the reference frames. The grey bars represent the time delay value in the feedback-control loop, which is the time between the sampling time of state signals and the effecting time of control signals. The results show that the loop time delay with the traditional scheme is about 40ms, and the loop time delay with the proposed scheme is less than 10ms. The proposed approach can significantly reduce the time delay of the feedback-control loop by 75%.

*B. Case studies*

To verify the effectiveness of the proposed method, three typical steering wheel angle inputs are considered in this study, including the ramp steering test, fishhook steering test and double lane-changing steering test. The respective steering wheel angle signals as shown in Fig. 9.

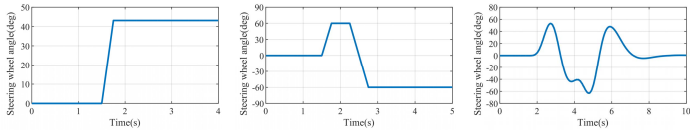


a. Steering wheel angle with Ramp test b. Steering wheel angle with Fishhook test c. Steering wheel angle with double-lane-change

Fig. 9 Three test cases

The proposed HSCF is compared with a traditional control one with time-driven mode without network scheduling or 'none network scheduling' (NNS). For a fair comparison, the same parameter values are set as follows: the system sampling period for the vehicle motion control system is set as $T$=0.02s, and the fixed step is selected for the solver in the simulator with 0.001s. The weighting matrices in the performance index of the linear quadratic regulator are chosen as:

$$Q=\begin{bmatrix} 20000 & 0 \\ 0 & 7500 \end{bmatrix}, \qquad R=0.000005$$

By using the lqrd command in MATLAB, the control gains $K$ matrix of the discrete-time linear quadratic regulator can be obtained as $K = [10899, 26315]$. Also, by using the LMI Toolbox in MATLAB, the control gains $K'$ matrix of the $H_\infty$-based linear quadratic regulator can be obtained as $K' = [9427, 21154, 0.086]$.

1) *Ramp steering test*

In this test, the vehicle longitudinal speed is set to be 100 km/h, and the tire-road friction coefficient is 0.85. As shown in Fig. 10.a, both the traditional NNS method and the proposed HSCF method can keep the actual yaw rate tracking the desired yaw rate well in the ideal simulation without the effects of the in-vehicle network. However, as shown in Fig.10.b, the real-time HIL test results with the in-network show that the traditional NNS method leads to the larger overshoot of yaw rate, which is about 17.6% and the longer response time, which is about 1.7s. Whereas the proposed HSCF method only brings about the overshoot of 8.8% and the response time of 0.65s, respectively. The results as in Fig.10.c show that the traditional method leads to the response distances of 46.8m in the longitudinal direction and 5.17m in the lateral direction in the transient state process of the yaw rate adjustment. Whereas the proposed method brings about the response distances of 18m in the longitudinal direction and 0.44m in the lateral direction. The results as in Fig.10.d show that the proposed HSCF method reduced the response distance by 61.5% in the vehicle yaw motion adjustment process, which means that the high-speed vehicle is faster and safer when cornering and overtaking with the HSCF. The results as in Fig. 10.e-h also show that the traditional NNS method leads to more oscillations in the torque outputs of four driving motors. It means serious damage and extra energy consumption for the driving motors, and even worse, safety and ride comfort of the vehicles with the traditional method. Whereas, with the proposed method, the vehicle yaw motion can be adjusted smoother and faster, which means that

This article has been accepted for publication in a future issue of this journal, but has not been fully edited. Content may change prior to final publication. Citation information: DOI 10.1109/TIE.2021.3070499, IEEE Transactions on Industrial Electronics



the vehicle is safer and more comfortable for drivers and passengers in the Ramp steering.

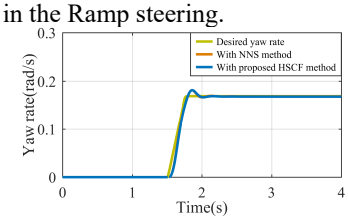


a.Yaw rate response results without the network effects

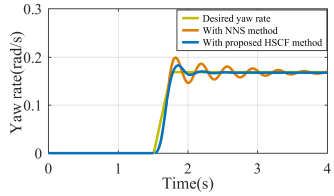


b.Yaw rate response results with the network effects

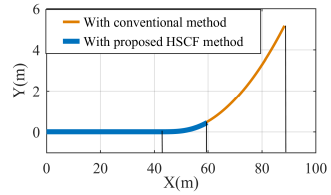


c. Response distances

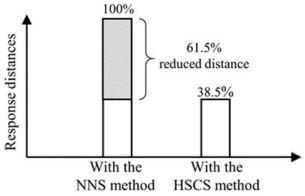


d. Comparative reduced distance

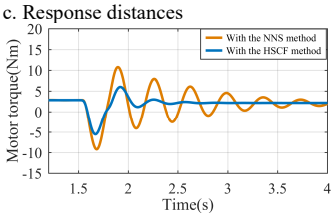


e. Motor torque of front left wheel

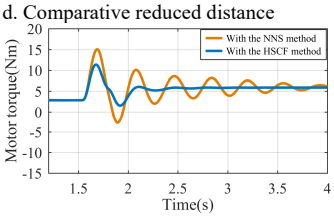


f. Motor torque of front right wheel

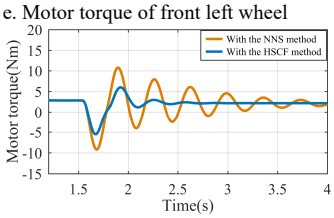


g. Motor torque of rear left wheel

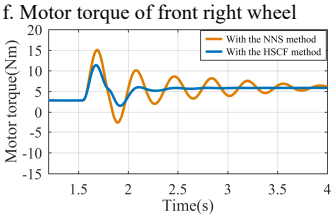


h. Motor torque of rear right wheel

Fig. 10 Ramp steering test

2) *Fishhook steering test*

In this test, the vehicle longitudinal speed is set as 80 km/h, and the tire-road friction coefficient is 0.85. Fig.11 shows the real-time HIL test results with the two designed methods in fishhook steering tests. It is obvious that the traditional NNS scheme leads more transient oscillations in the vehicle yaw-rate as in Fig.11b and even the periodic oscillation in the torque outputs of four driving motors as in Fig.11c-f. As a result, the vehicle system maybe at the edge of losing stability. Whereas the proposed HSCF has almost no negative influence on the vehicle yaw motion tracking performance and the torque outputs of the driving motors.

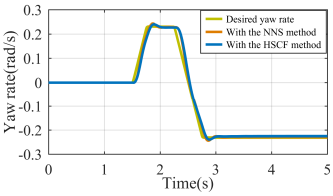


a. Yaw rate response results without the network effects

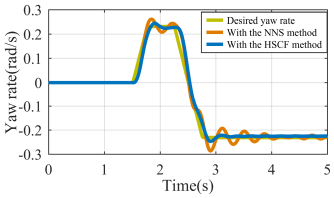


b.Yaw rate response results with the network effects

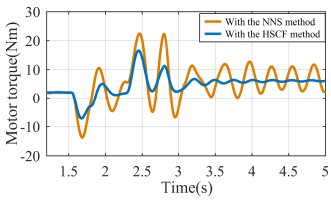


c. Motor torque of front left wheel

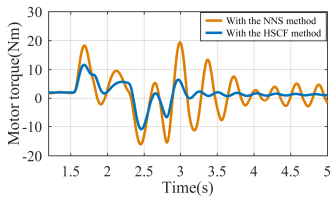


d. Motor torque of front right wheel

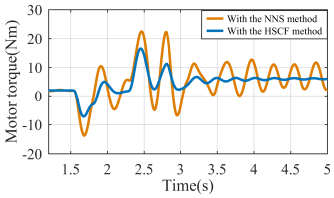


e. Motor torque of rear left wheel

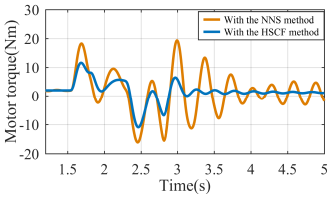


f. Motor torque of rear right wheel

Fig. 11. Fishhook steering tests.

3) *Double-lane-change steering test*

In the third case, the double lane-changing steering is tested. In this test, the vehicle longitudinal speed is set to be 100 km/h, and the tire-road friction coefficient is 0.85. The comparative results are shown in Fig. 12. They are showing almost the same performance with the previous two tests. Under the real-time networked control environment, with the traditional NNS scheme, there are more significant transient oscillations. Whereas with the proposed HSCF, it is able to guarantee the satisfactory motion control performance and robust stability in spite of the network effects, which illustrate the strength of explicitly dealing with in-vehicle network effects.

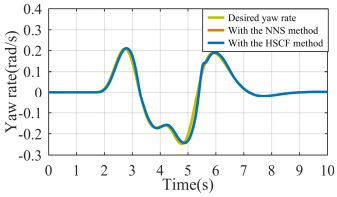


a. Yaw rate response results without the network effects

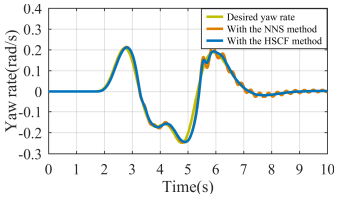


b.Yaw rate response results with the network effects

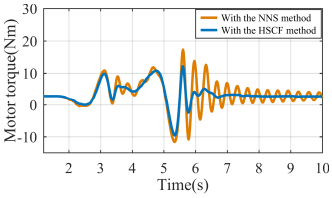


c. Motor torque of front left wheel

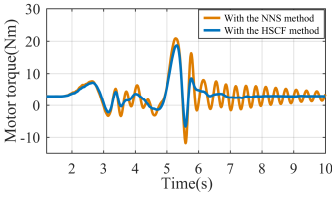


d. Motor torque of front right wheel

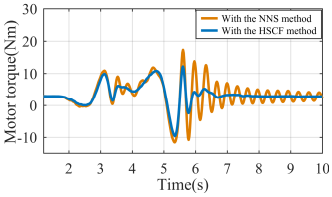


e. Motor torque of rear left wheel

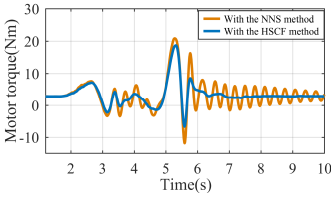


f. Motor torque of rear right wheel

Fig. 12. Double-lane-change steering tests.

## C. Comparison studies

For comparison studies of the proposed scheduler and controller, the effects of four cases are tested respectively. The four cases are as follows in Table II:

TABLE II. COMPARISON CASES

| | |
|---|---|
| *Case 1* | LQR control without multiple-package transmissions scheduler |
| *Case 2* | LQR control with multiple-package transmissions scheduler |
| *Case 3* | Robust control without multiple-package transmissions scheduler |
| *Case 4* | Robust control with multiple-package transmissions scheduler |

In this test, the steering wheel angle input adopted a ramp steering manoeuvre. The vehicle longitudinal speed is set to be 100 km/h, and the tire-road friction coefficient is 0.85. Two system sampling periods (T=0.02s and T=0.04s) are considered in this test.

This article has been accepted for publication in a future issue of this journal, but has not been fully edited. Content may change prior to final publication. Citation information: DOI 10.1109/TIE.2021.3070499, IEEE Transactions on Industrial Electronics



When T=0.02s, the *Case 1* leads to the larger overshoot of yaw rate and longer response time in the transient process as shown in Fig. 13. a. *Case 2* and *Case 3* could reduce the overshoot and response time, highlighting the effect of multiple-package transmissions scheduler and the robust controller to some extent. The *Case 4* keeps the best tracking of the desired yaw rate and leads to the shortest response time.

When T=0.04s, as shown in Fig.13.b, it is obvious that the *Case 1* lead to periodic oscillation in the vehicle yaw-rate. *Case 2* and *Case 3* could track the desired yaw rate but fail in the overall system performance with larger overshoot and longer response. Whereas the *Case 4* has almost no negative influence on the vehicle yaw motion tracking performance. These results show that the proposed HSCF scheme is more effective than the ones with MPT, robust $H_\infty$-*LQR* controller or traditional LQR controller.

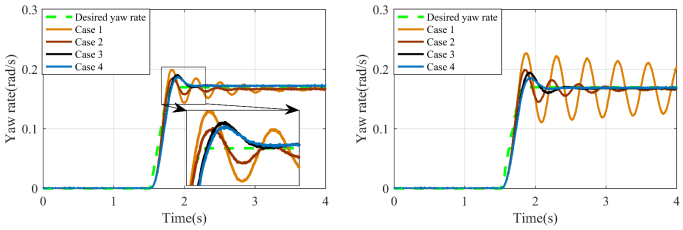


a. Yaw rate response results when T is 0.02s. b. Yaw rate response results when T is 0.04s.

Fig. 13. Comparison of yaw rate response results.

## V. CONCLUSIONS

The network motion control design for the EVs is a key challenging problem due to the non-synchronous multiple-package transmissions and time-varying network-induced delays, which will adversely weaken the vehicle stabilization and make the vehicle motion controller design difficult. This study proposes an HSCF, where the new developed scheduler approach is used to reorganize information flows; meanwhile the robust controller approach is designed to generate motion control commands and guarantee the system's robust stability. The real-time HIL bed test experimental results show that the proposed hybrid scheme and approaches could effectively improve the vehicle motion control performance and guarantee the robustness of the in-vehicle networked system. Nowadays, with the new networked electronic and electrical architecture (N-EEA), smarter vehicles with growing ADASs are being developed rapidly. The proposed hybrid framework and approaches can be potentially used in other related areas, which may also be worth of investigating in the future.

## APPENDIX A

The specifications of the four-in-wheel motors in a prototype Beijing Electric Vehicle Co., Ltd. used for simulation is shown as follows.

Table A. The four-in-wheel motors specifications.

| Symbol | Description | Value/Unit |
|---|---|---|
| $P_{Max}/P_R$ | MAX Power/Rated Power | 30kW/15kW |
| $\omega_{Max}/\omega_R$ | MAX Speed/Rated Speed | 9000rpm/3000rpm |
| $T_{Max}/T_R$ | MAX Torque/Rated Speed | 100Nm/50Nm |
| U | Operating Voltage for MCU | 300V-400V |
| I | Operating Voltage for MCU | 0A-120A |

## APPENDIX B

*Proof* of *Lemma 1:*

For a closed-loop system as in (B.1):

$$\begin{cases} x(k+1) = A_c x(k) + B_2 \omega(k) \\ z(k) = C_c x(k) + D_2 \omega(k) \end{cases} \tag{B.1}$$

According to Lyapunov stability theorem, the closed-loop system ~~(B.3)~~ (B.1) is stable with a given $H_\infty$ performance $\eta$, if there exists a positive definite matrix $P = P^T > 0$ satisfying.

$$\begin{aligned} &A_c^T P A_c - P - C_c^T C_c + \\ &\left(A_c^T P B_2 + C_c^T D_2\right)\left[\eta^2 I - \left(B_2^T P B_2 + D_2^T D_2\right)\right]^{-1}\left(B_2^T P A_c + D_2^T C_c\right) < 0 \\ &\eta^2 I - \left(B_2^T P B_2 + D_2^T D_2\right) < 0 \end{aligned} \tag{B.2}$$

With the Schur Complement, the functions (B.2) is equal to the function as following:

$$\begin{bmatrix} -P^{-1} & 0 & A_c & B_2 \\ 0 & -I & C_c & D_2 \\ A_c^T & C_c^T & -P & 0 \\ B_2^T & D_2^T & 0 & -\eta^2 I \end{bmatrix} < 0 \tag{B.3}$$

Then multiplying (B.3) by diag{P, I, I, I} on the left and by diag{*P, I, I, I*} on the right respectively, (B.3) can be transformed into (B.4).

$$\begin{bmatrix} -P & 0 & PA_c & PB_2 \\ 0 & -I & C_c & D_2 \\ A_c^T P & C_c^T & -P & 0 \\ B_2^T P & D_2^T & 0 & -\eta^2 I \end{bmatrix} < 0 \tag{B.4}$$

The system (20) is a special case of system (B.1), where

$$\begin{aligned} A_c &= A_{aug} - B_{aug} K^{'} \\ B_2 &= G_{aug} \\ C_c &= F - H K^{'} \\ D_2 &= 0 \end{aligned} \tag{B.5}$$

Substituting (B.5) into (B.4), the closed-loop system (20) is stable with a given $H_\infty$ performance $\eta$, if there exists a positive definite matrix $P = P^T > 0$, satisfying:

$$\begin{bmatrix} -P & 0 & P\left(A_{aug} - B_{aug} K^{'}\right) & PG_{aug} \\ 0 & -I & F - H K^{'} & 0 \\ A_{aug}^T P^T - K^{'T} P^T B_{aug}^T & F^T - K^{'T} H^T & -P & 0 \\ G_{aug}^T P^T & 0 & 0 & -\eta^2 I \end{bmatrix} < 0 \tag{B.6}$$

The *lemma 1* is proved.

## REFERENCES

[1] W. Wang, C. Zhang, J. Wang *et al.*,-"Multi-purpose flexible positioning device based on electromagnetic balance for EVs wireless charging," *IEEE Transactions on Industrial Electronics*, pp. 1-1, 2020.

[2] M. Xiong, X. Wei, Y. Huang *et al.*, "Research on novel flexible high-saturation nanocrystalline cores for wireless charging systems of electric vehicles," *IEEE Transactions on Industrial Electronics*, pp. 1-1, 2020.

[3] R. Wang, H. Jing, F. Yan *et al.*, "Optimization and finite-frequency H-infinity control of active suspensions in in-wheel motor driven electric ground vehicles," *Journal of the Franklin Institute-Engineering and Applied Mathematics,* vol. 352, no. 2, pp. 468-484, 2015.

[4] S. De Pinto, P. Camocardi, A. Sorniotti *et al.*, "Torque-fill control and energy management for a four-wheel-drive electric vehicle layout with two-speed transmissions," *IEEE Transactions on Industry Applications,* vol. 53, no. 1, pp. 447-458, 2017.

[5] Y. Wang, H. Fujimoto, and S. Hara, "Driving force distribution and control for EV with four in-wheel motors: A case study of acceleration on split-friction surfaces," *IEEE Transactions on Industrial Electronics,* vol. 64, no. 4, pp. 3380-3388, 2017.

[6] J. Zhao, J. Chen, and C. Liu, "Stability coordinated control of distributed drive electric vehicle based on condition switching," *Mathematical Problems in Engineering,* vol. 2020, 2020.

[7] D. Savitski, V. Ivanov, K. Augsburg *et al.*, "Wheel slip control for the electric vehicle with in-wheel motors: Variable structure and sliding mode methods," *IEEE Transactions on Industrial Electronics,* vol. 67, no. 10, pp. 8535-8544, 2020.

[8] Z. Li, L. Zheng, W. Gao *et al.*, "Electromechanical coupling mechanism and control strategy for in-wheel-motor-driven electric vehicles," *IEEE Transactions on Industrial Electronics,* vol. 66, no. 6, pp. 4524-4533, 2019.

[9] Y. Jang, M. Lee, I.-S. Suh *et al.*, "Lateral handling improvement with dynamic curvature control for an independent rear wheel drive EV," *International Journal of Automotive Technology,* vol. 18, no. 3, pp. 505-510, 2017.

[10] L. Xiong, G. W. Teng, Z. P. Yu *et al.*, "Novel stability control strategy for distributed drive electric vehicle based on driver operation intention," *International Journal of Automotive Technology,* vol. 17, no. 4, pp. 651-663, 2016.

[11] J. Guo, Y. Luo, K. Li *et al.*, "Coordinated path-following and direct yaw-moment control of autonomous electric vehicles with sideslip angle estimation," *Mechanical Systems and Signal Processing,* vol. 105, pp. 183-199, 2018.

[12] Y. H. Shen, Y. Gao, and T. Xu, "Multi-axle vehicle dynamics stability control algorithm with all independent drive wheel," *International Journal of Automotive Technology,* vol. 17, no. 5, pp. 795-805, 2016.

[13] W. Zhao, Q. Song, W. Liu *et al.*, "Distributed electric powertrain test bench with dynamic load controlled by neuron PI speed-tracking method," *IEEE Transactions on Transportation Electrification,* vol. 5, no. 2, pp. 433-443, ~~Jun~~ 2019.

[14] M. Wein, C. Graf, S. Strasser *et al.*, "The electric all-wheel drive in the Audi e-tron," *ATZ worldwide,* vol. 121, no. 6, pp. 16-21, 2019.

[15] L. Jian,-"Research status and development prospect of electric vehicles based on hub motor," *2018 china international conference on electricity distribution*, China international conference on electricity distribution, pp. 126-129, New York: IEEE, 2018.

[16] L. Guo, P. Ge, M. Yue *et al.*, "Trajectory tracking algorithm in a hierarchical strategy for electric vehicle driven by four independent in-wheel motors," *Journal of the Chinese Institute of Engineers,* vol. 43, no. 8, pp. 807-818, 2020.

[17] L. Guo, H. Xu, J. Zou *et al.*, "Variable gain control-based acceleration slip regulation control algorithm for four-wheel independent drive electric vehicle," *Transactions of the Institute of Measurement and Control*, 2020.

[18] H. N. Peng, W. D. Wang, C. L. Xiang *et al.*, "Torque coordinated control of four in-wheel motor independent-drive vehicles with consideration of the safety and economy," *IEEE Transactions on Vehicular Technology,* vol. 68, no. 10, pp. 9604-9618, 2019.

[19] S. A. Mortazavizadeh, A. Ghaderi, M. Ebrahimi *et al.*, "Recent developments in the vehicle steer-by-wire system," *IEEE Transactions on Transportation Electrification*, 2020.

[20] H. Zhao, C. Liu, Z. Song *et al.*, "Analytical modelling of a double-rotor multi-winding machine for hybrid aircraft propulsion," *IEEE Transactions on Transportation Electrification*, 2020.

[21] Z. Shuai, H. Zhang, J. Wang *et al.*, "Combined AFS and DYC control of four wheel independent drive electric vehicles over CAN network with time-varying delays," *IEEE Transactions on Vehicular Technology,* vol. 63, no. 2, pp. 591-602, 2014.

[22] G. Qin, and J. Zou, "$H_\infty$ control of four wheel independent drive electric vehicles with random time-varying delays," *Mathematical Problems in Engineering,* vol. 245493, 2015.

[23] J. Ni, J. B. Hu, and C. L. Xiang, "Envelope control for four-wheel independently actuated autonomous ground vehicle through AFS/DYC integrated control," *IEEE Transactions on Vehicular Technology,* vol. 66, no. 11, pp. 9712-9726, 2017.

[24] S. Inoue, T. Nasu, T. Hayashi *et al.*, "A shared-control-based driver assistance system using steering guidance torque combined direct yaw-moment control", *Dynamics of Vehicles on Roads and Tracks,* Vol 1. 2018, pp. 135-140.

[25] H. Zhang, Y. Shi, J. M. Wang et al., "A new delay-compensation scheme for networked control systems in controller area networks," *IEEE Transactions on Industrial Electronics*, vol. 65, no. 9, pp. 7239-7247, 2018.

[26] X. Zhu, H. Zhang, J. Wang *et al.*, "Robust lateral motion control of electric ground vehicles with random network-induced delays," *IEEE Transactions on Vehicular Technology,* vol. 64, no. 11, pp. 4985-4995, 2015.

[27] W. Cao, Y. Wu, E. Zhou *et al.*, "Reliable integrated ASC and DYC control of all-wheel-independent-drive electric vehicles over CAN using a co-design methodology," *IEEE Access,* vol. 7, pp. 6047-6059, 2019.

[28] D. Patil, M. K. McDonough, J. M. Miller *et al.*, "Wireless power transfer for vehicular applications: Overview and challenges," *IEEE Transactions on Transportation Electrification,* vol. 4, no. 1, pp. 3-37, 2017.

[29] Z. Shuai, H. Zhang, J. Wang *et al.*, "Lateral motion control for four-wheel-independent-drive electric vehicles using optimal torque allocation and dynamic message priority scheduling," *Control Engineering Practice,* vol. 24, pp. 55-66, 2014.

[30] W. Cao, Z. Liu, Y. Chang *et al.*, "Direct yaw-moment control of all-wheel-independent-drive electric vehicles with network-induced delays through parameter-dependent fuzzy SMC approach," *Mathematical Problems in Engineering,* vol. 5170492, 2017.

[31] W. Li, W. Zhu, X. Y. Zhu *et al.*, "Torsional oscillations control of integrated motor-transmission system over controller area network," *Ieee Access,* vol. 8, pp. 4397-4407, 2020.

[32] X. M. Li, Y. Chen, and J. Y. Li, "Finite-time state estimation for delayed periodic neural networks over multiple-packet transmission," *Neurocomputing,* vol. 311, pp. 137-145, 2018.

[33] H. B. Li, H. J. Yang, F. C. Sun *et al.*, "Sliding-mode predictive control of networked control systems under a multiple-packet transmission policy," *IEEE Transactions on Industrial Electronics,* vol. 61, no. 11, pp. 6234-6243, 2014.

[34] J.-S. Hu, D. Yin, Y. Hori *et al.*, "Electric vehicle traction control: A new MTTE methodology," *IEEE Industry Applications Magazine,* vol. 18, no. 2, pp. 23-31, 2012.

[35] Y. Shi, J. Huang, and B. Yu, "Robust tracking control of networked control systems: Application to a networked dc motor," *IEEE Transactions on Industrial Electronics*, vol. 60, no. 12, pp. 5864-5874, 2013.

[36] J. R. Pimentel, and J. A. Fonseca, "Flexcan: A flexible architecture for highly dependable embedded applications, rtn2004.," in Third International Workshop on Real-Time Networks, Catania, Italy, 2004.

[37] W. K. Cao, H. L. Liu, C. Lin *et al.*, "Co-design based lateral motion control of all-wheel-independent-drive electric vehicles with network congestion," *Energies,* vol. 10, no. 10, pp. 16, 2017.

[38] Kumar, B. Vinodh, and J. Ramesh. "Improved Automotive CAN Protocol Based on Payload Reduction and Selective Bit Stuffing." Circuits and Systems 3415-3429, 7(10), 2016.

[39] H. Zhang, Y. Shi, and B. X. Mu, "Optimal H-infinity-based linear-quadratic regulator tracking control for discrete-time takagi-sugeno fuzzy systems with preview actions," *Journal of Dynamic Systems Measurement and Control-Transactions of the Asme,* vol. 135, no. 4, pp. 5, 2013.


Wanke Cao (M'18) received the B.S. degree in Mechanical Engineering and Automation, and the Ph.D. degree in Vehicle Engineering from Northeastern University, Shenyang, China, in 2003 and 2008, respectively. From 2008 to 2010, he was a Postdoctoral Researcher with the Department of Vehicle Engineering, Beijing Institute of Technology, Beijing. He was a Visiting Scholar with the Department of Multisource Propulsion Systems, Warsaw University of Technology, Warsaw, Poland. Since 2018, He has been an Associate Professor with the National Engineering Laboratory for Electric Vehicles and the School of Mechanical Engineering, Beijing Institute of Technology. His current research interests include vehicle dynamics and control, networked control, in-vehicle network, communication protocol, motion control, and robust control for electric vehicles.

Jizhi Liu was born in Enshi, Hubei province, China in 1995. He received the B.E. degree in military vehicle engineering from the Beijing Institute of Technology, in 2018. He is currently a graduate student with the Department of Vehicle Engineering, Beijing Institute of Technology. His current research interests include the net-worked control of electric vehicles and the in-vehicle network technology.

Jianwei Li (M'19) received the B.Eng. degree from North China Electric Power University. He received the M.Sc. degree in Power System and the Ph.D. degree in Electrical Engineering from the University of Bath, U.K. He has worked with the University of Liege, Beijing Institute of Technology and University of Oxford. His research interests include electrical energy storages and hybrid energy storages, electrical vehicles, networked control of electric vehicles.

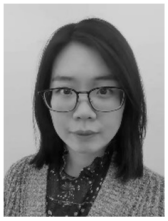

Qingqing Yang (S'14, M'17) received Ph.D. degree from the University of Bath, U.K. She worked as a Lead Engineer on the electrical engineering when she was in the Beijing Electric Power Research Institute, State Grid Corporation of China. She is currently a Lecture with Coventry University. Her research interests include HVDC control and protection, virtual inertia in the power systems and artificial intelligence applications in energy storage, and smart grids.

Hongwen He (M'03–SM'12) received the M.Sc. degree from the Jilin University of Technology, Changchun, China, in 2000 and the Ph.D. degree from the Beijing Institute of Technology, Beijing, China, in 2003, both in vehicle engineering. He is currently a Professor with the National Engineering Laboratory for Electric Vehicles, Beijing Institute of Technology. His research interests include power battery modeling and simulation on electric vehicles, design, and control theory of the hybrid power trains.